American Mineralogist, Volume 81, pages 928–939, 1996

Mutual exsolution in hornblende and cummingtonite: Compositions, lamellar orientations, and exsolution temperatures

ULRICH KLEIN,[1,*] JOHN C. SCHUMACHER,[1] AND MICHAEL CZANK[2]

[1]Institut für Mineralogie, Petrologie und Geochemie der Albert-Ludwigs-Universität zu Freiburg, Albertstrasse 23b, 79104 Freiburg, Germany

[2]Mineralogisch-Petrographisches Institut der Christian-Albrechts Universität zu Kiel, Olshausenstrasse 40, 24098 Kiel, Germany

ABSTRACT

Exsolved pairs of hornblende and cummingtonite from two localities in southern New England, U.S.A., have been studied using transmission electron microscopy (TEM) to measure the crystallographic orientation of the exsolution lamellae. Both the cummingtonite and the hornblende show multiple generations or stages of exsolution. Electron microprobe analyses gave compositions of the pre-exsolved (averages) and the coarsest exsolved amphiboles.

In amphiboles, two orientations of lamellae are usually present and nearly parallel to {100} and {10$\bar{1}$} of the host. The observed lamellar orientations are consistent with orientations predicted by the optimal phase-boundary (OPB) theory and are a function of small differences in a, c, and β of the host and exsolved amphiboles ($\Delta a = a_{host} - a_{lamella}$, $\Delta\beta = \beta_{host} - \beta_{lamella}$, and $\Delta c = c_{host} - c_{lamella}$). Because these lattice parameters vary with T and composition, the precise orientations of the lamellae are controlled by these variables. The widths of determined exsolution lamellae varied from microscopic (micrometer size) to submicroscopic (nanometer size). The TEM images show, in some cases, multiple generations of lamellae with lamellar orientations near {10$\bar{1}$} differing up to 4.1°, whereas orientations near {100} differed up to 4°. For two pairs of coexisting amphiboles, the T dependence of the lattice parameters from 25 to 600 °C was measured using a Guinier camera. The OPB calculations indicate that for all the samples the different lamellar generations formed between about 780 and 300 °C (±80 °C, on the basis of maximum errors of the lattice-parameter determinations). Lamellae of the same generation all showed nearly the same width. Exsolution temperatures could not be derived from the "100" lamellae because relatively small variations in Δc, which controls exact orientation of the "100" lamellae, could not be measured accurately enough.

INTRODUCTION

A miscibility gap between the clinoamphiboles cummingtonite and hornblende was first proposed by Asklund (1923) and verified in 1962 (Asklund et al. 1962). Numerous workers have reported exsolution phenomena in coexisting cummingtonite and hornblende in amphibolite rocks from diverse geologic settings (e.g., Seitasaari 1952; Vernon 1962; Robinson 1963; Binns 1965; Boriani and Minutti 1965; Calleghari 1966; Jaffe et al. 1968; reviewed in Robinson et al. 1982a). In clinoamphiboles (space group $C2/m$), the host and the exsolved phases were commonly thought to share the {100} or {10$\bar{1}$} planes. Using X-ray data, Ross et al. (1969) and Robinson and Jaffe (1969) found discrepancies between the actual and assumed lamellar orientations but could not interpret them. Later, Robinson et al. (1971) showed that these phase boundaries are not exactly parallel to the {100} or {10$\bar{1}$} planes but are actually irrational planes close to {100} or {10$\bar{1}$}. In the present study, these plane orientations are designated as "100" and "10$\bar{1}$". Bollman and Nissen (1968) termed such irrational planes the optimal phase boundaries. The "100" and "10$\bar{1}$" orientations correspond to a minimum of lattice misfit and interfacial energy. Assuming nearly identical b lattice parameters for two intergrown phases, Robinson et al. (1971, 1977) showed that in hornblende-cummingtonite and augite-pigeonite pairs the orientations of exsolution lamellae are restricted to two exact phase boundaries in the a-c plane. These exact phase boundaries correspond to two vectors in the a-c planes of each lattice and that have the same lengths (see appendix of Robinson et al. 1977). The lengths of the vectors and, therefore, the orientations of these boundaries are functions of the differences in the lattice parameters (Δa, Δc, and $\Delta\beta$) of the amphibole lamellae and host. Further discussion of optimal phase-boundary theory and application of the theory to other minerals can be found in Fleet (1982, 1985).

* Present address: Mineralogisch-Petrographisches Institut der Christian-Albrechts Universität zu Kiel, Olshausenstrasse 40, 24098 Kiel, Germany.

0003–004X/96/0708–0928$05.00

Recent work by Yang and Hirschmann (1995) suggests that Mg-rich clinoamphiboles, like the clinopyroxenes, show a phase transition from the *C*-centered to the primitive monoclinic unit cell in compositions at geologically relevant temperatures. However, in comparison with pyroxenes, there are much smaller changes in the amphibole lattice parameters both as a result of the phase transition and as a function of temperature (for pyroxenes, see Smith 1969, Cameron et al. 1973, Smyth 1974, Robinson et al. 1977; for amphiboles, see Cameron and Papike 1979, Yang and Hirschmann 1995). The exsolution processes in both mineral pairs are analogous, but because of the conversions used to assign group designations (*I2/m* vs. *C2/m*) the approximate orientations of the exsolution planes are indexed differently: near {100} and {001} in augite and pigeonite, and near $\{10\bar{1}\}$ and {100} in hornblende and cummingtonite. The amphiboles that were studied here have space group *C2/m*. Discussion of the relationships between the *C2/m* unit-cell setting and the *I2/m* unit-cell setting can be found in Whittaker and Zussman (1961), Jaffe et al. (1968), Thompson (1978), and Robinson et al. (1982a, p. 60, Fig. 26).

Robinson et al. (1977) devised a geothermometer for exsolved monoclinic pyroxenes (augite and pigeonite) on the basis of the orientation of the exsolution lamellae and Fe-Mg content. The present study aims to determine if exsolved cummingtonite and hornblende can also be used as a geothermometer that would give temperatures of exsolution.

Geologic setting of samples

The exsolved cummingtonite and hornblende that were used in this study are from the amphibolites of Middle Ordovician rocks of the Partridge Formation and the Ammonoosuc Volcanics (Schumacher 1988; Hollocher 1993) from central Massachusetts and southwestern New Hampshire (Fig. 1). Metamorphism and structural development of this region occurred mainly during the Devonian Acadian orogeny, during which plutonism, nappe-style tectonism, and syntectonic metamorphism that was followed by the formation of gneiss domes all occurred (e.g., Robinson 1986; Robinson et al. 1986, 1991).

Sample localities (Fig. 1) lay (1) within the Bronson Hill anticlinorium along the Massachusetts–New Hampshire border (samples 7A7C, 7A7D, 7A7R, and 7A7W, referred to here as the 7A7 series) and (2) on the eastern flank of the Bronson Hill anticlinorium in central Massachusetts (samples Q-603C, Q-798M, Q-J44R, WD-N27A, WD-H26C, and HFW-307W, designated as the CM series). For the rocks of the 7A7 series, the pelitic schists in this area yielded temperature estimates of 550–640 °C on the basis of garnet-biotite geothermometry (Tracy et al. 1976) and a minimum pressure estimate of 5–6.2 kbar on the basis of quartz + sillimanite + garnet assemblages (Robinson et al. 1982b). Peak metamorphic conditions for the CM series range between 635 and 675 °C and at least 5.5 and 7.2 kbar (Hollocher 1985).

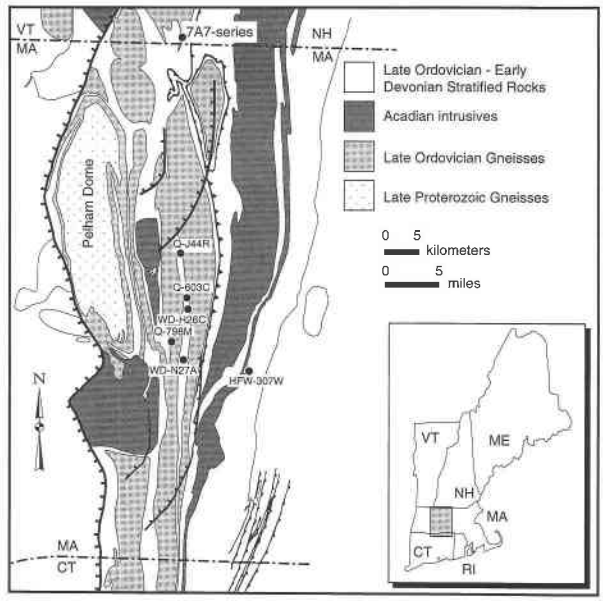

Figure 1. Generalized geologic map of central Massachusetts and southwestern New Hampshire that shows the locations of the sample localities (geology after Robinson et al. 1982b).

Experimental techniques

The amphiboles were studied using transmission electron microscopy (TEM) and electron microprobe (EMP) analysis at Kiel University. The TEM samples were drilled out of standard petrographic thin sections with the use of an ultrasonic disc cutter and prepared by ion milling. Electron microscopy was performed with a Philips EM400T operating at 100 kV and equipped with an energy-dispersive X-ray analyzing system (Kevex, Unispec System 7000).

Heating experiments were performed with a Guinier film camera (Huber) at 50 kV and 20 mA using Cu$K\alpha_1$ radiation. For Guinier camera measurements, amphibole powder was placed in quartz capillaries, which were closed after filling to minimize the amphibole oxidation and measured at various temperatures up to about 600 °C. Note that the prismatic habit of amphiboles led to their partial preferred orientation which reduced the accuracy of *c*-axis determinations. An internal silicon standard was used to correct for film shrinkage. *T*-dependent lattice parameters were determined by least-squares using the computer program FINAX (Hovestreydt 1983). For each sample, 11 reflections were used for lattice-parameter determination. Quantitative chemical analyses of amphibole were performed on a Camebax-MBX (Cameca) electron microprobe operated at 15 kV and 15 mA. Natural mineral standards were used.

Mineral compositions

The minerals of the assemblages were analyzed with the EMP. The EMP work concentrated on (1) the amphibole bulk chemistry and (2) the compositions of the coarsest exsolved end-members. In all ten samples the

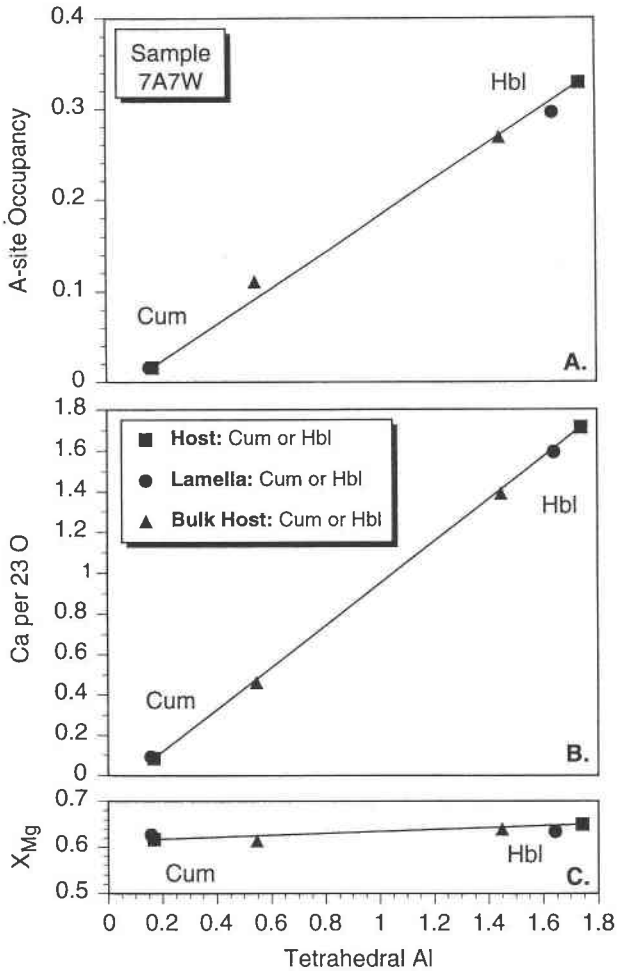

FIGURE 2. Three chemical plots of coexisting clinoamphiboles (sample 7A7W). (**A**) $^{[4]}$Al vs. A-site occupancy, (**B**) $^{[4]}$Al vs. Ca per 23 O atoms, and (**C**) $^{[4]}$Al vs. X_{Mg}. The bulk compositions of the host phases are averages of 60–70 electron microprobe point analyses across a single grain. Host and lamellar compositions were averages of 10–15 point analyses.

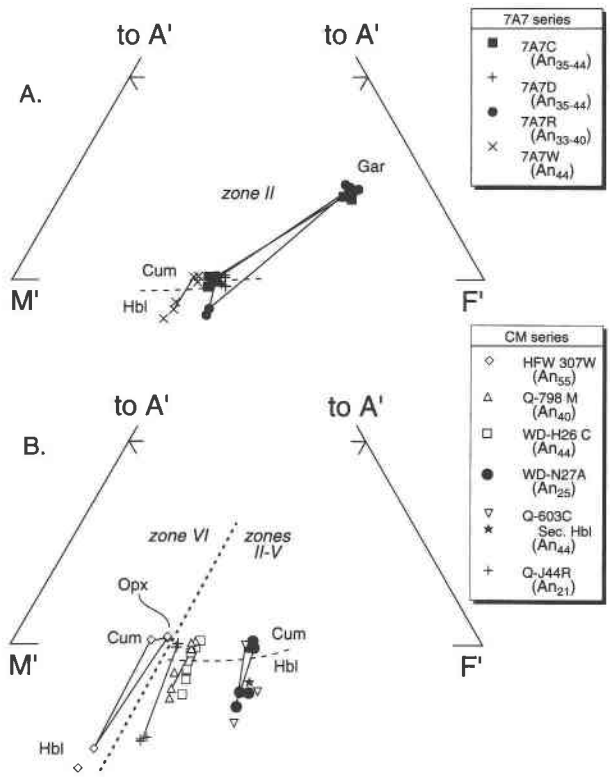

FIGURE 3. Ternary plot of the compositions of coexisting phases in samples from the (**A**) 7A7 series and (**B**) CM series. The diagram is a projection from plagioclase, quartz, and water. Coordinates: A′ = Al_2O_3 + Fe_2O_3 + TiO_2 − Na_2O − CaO, M′ = MgO, and F′ = FeO + MnO − TiO_2.

bulk amphibole compositions were calculated from 60 to 90 point analyses collected in 1 μm steps across the grain perpendicular to one set of lamellae. These point analyses are mostly overlapping analyses. Because the diameter of the electron beam was about 2 μm, only coarser exsolution lamellae could be measured. About 10–20 point analyses were taken to get an average composition of the more coarsely exsolved amphibole.

Ferric estimates

Because of the fine scale of the exsolution, Mössbauer and wet-chemical analysis for amphibole Fe^{3+} contents were not possible. Estimates of Fe^{3+} contents for optically homogeneous cummingtonite samples were obtained by normalizing the sum of cations, excluding Na and K, to 15 [15eNK; see also Stout (1972), Robinson et al. (1982a, p. 3–12), and Schumacher (1991) for discussion]. For optically homogeneous hornblende, normalizing the cation sum, excluding Ca, Na, and K, to 13 (13eCNK) yields the maximum ferric estimate but precludes the presence of cummingtonite component. Because these hornblendes coexist with cummingtonite, this procedure certainly overestimates the ferric content of the hornblende. Alternatively, the 15eNK correction gives a minimum Fe^{3+} estimate, but, on the basis of Fe-Mg partitioning with cummingtonite, the 15eNK correction appears to be too conservative. By varying the amounts of Na that were assigned to the M4 position, it was possible to arrive at formulas that gave reasonable Fe-Mg values, Na content at M4, and cummingtonite contents.

Mineral assemblages and compositions

In addition to the exsolved hornblende and cummingtonite, all samples bore plagioclase, biotite, and quartz. Samples 7A7R and 7A7C (Fig. 1) also contained garnet. In sample HFW-307W, orthopyroxene was present.

Figure 2 shows $^{[4]}$Al plotted against A-site occupancy (Fig. 2A), Ca per 23 O atoms (Fig. 2B), and X_{Mg} for cummingtonite and hornblende in sample 7A7W (Fig. 2C) (see Table 1). Each plot suggests Fe^{3+} correction is reasonable because in each case all six data points lie essentially on the tie line connecting the exsolved amphibole end-members.

The microprobe data for all the analyzed amphiboles are compared in AFM diagrams (Fig. 3). Plagioclase in

TABLE 1. Microprobe data and calculated amphibole formula of samples 7A7W and Q-603C

	7A7W						Q-603C					
	Host Cum	Lamella Hbl	Bulk host Cum	Host Hbl	Lamella Cum	Bulk host Hbl	Host Cum	Lamella Hbl	Bulk host Cum	Host Hbl	Lamella Cum	Bulk host Hbl
SiO_2	54.60	43.60	51.68	42.90	54.76	45.07	52.66	44.62	52.02	43.38	47.79	44.02
TiO_2	0.06	1.06	0.30	1.05	0.06	0.87	0.10	0.88	0.19	1.11	0.57	1.11
Al_2O_3	0.80	13.07	4.04	13.79	0.82	11.42	1.27	11.38	2.38	12.76	7.66	12.03
Cr_2O_3	0.01	0.02	0.01	0.01	0.01	0.01	0.01	0.01	0.01	0.01	0.00	0.01
FeO	22.72	17.00	21.28	16.34	21.97	17.57	27.47	20.67	26.98	18.34	22.76	18.89
MnO	0.88	0.34	0.76	0.35	0.92	0.46	0.37	0.18	0.34	0.13	0.25	0.15
MgO	19.21	10.92	17.07	10.56	19.56	12.19	15.25	9.38	14.54	8.92	12.15	9.35
CaO	0.55	10.19	2.99	10.95	0.61	8.93	0.88	8.99	1.65	11.15	6.14	10.55
Na_2O	0.06	1.54	0.47	1.69	0.05	1.39	0.12	1.32	0.26	1.41	0.87	1.36
K_2O	0.00	0.30	0.08	0.32	0.01	0.27	0.02	0.32	0.04	0.49	0.30	0.49
Total	98.89	98.05	98.67	97.95	98.77	98.15	98.14	97.75	98.41	97.71	97.51	97.96
wt% H_2O*	2.09	2.06	2.08	2.05	2.09	2.06	2.02	2.01	2.02	2.02	2.03	2.02
Full total	101.14	100.75	100.99	100.70	100.89	100.81	100.26	99.97	100.48	100.05	99.80	100.29
Si	7.861	6.358	7.448	6.259	7.861	6.551	7.805	6.663	7.706	6.453	7.051	6.535
$^{[4]}Al$	0.136	1.642	0.552	1.741	0.139	1.449	0.195	1.337	0.294	1.547	0.949	1.465
Total T	7.997	8.000	8.000	8.000	8.000	8.000	8.000	8.000	8.000	8.000	8.000	8.000
$^{[6]}Al$	0.000	0.603	0.134	0.630	0.000	0.507	0.027	0.666	0.121	0.690	0.382	0.640
Ti	0.006	0.117	0.033	0.115	0.006	0.095	0.011	0.099	0.021	0.124	0.063	0.124
Cr	0.001	0.002	0.001	0.001	0.001	0.001	0.001	0.001	0.001	0.002	0.000	0.002
Fe^{3+}	0.000	0.704	0.298	0.759	0.034	0.649	0.108	0.241	0.047	0.367	0.279	0.339
Mg	4.123	2.375	3.667	2.296	4.186	2.642	3.370	2.087	3.212	1.977	2.673	2.070
Fe	0.870	1.199	0.867	1.199	0.773	1.106	1.483	1.906	1.598	1.840	1.603	1.825
Total M1–M3	5.000	5.000	5.000	5.000	5.000	5.000	5.000	5.000	5.000	5.000	5.000	5.000
Fe	1.866	0.171	1.399	0.035	1.830	0.381	1.814	0.434	1.697	0.075	0.925	0.182
Mn	0.107	0.042	0.093	0.043	0.112	0.057	0.046	0.023	0.042	0.017	0.031	0.019
Ca	0.085	1.593	0.462	1.712	0.094	1.391	0.140	1.438	0.260	1.780	0.970	1.680
Na	0.000	0.194	0.046	0.210	0.000	0.171	0.000	0.105	0.001	0.128	0.074	0.119
Total M4	2.058	2.000	2.000	2.000	2.036	2.000	2.000	2.000	2.000	2.000	2.000	2.000
Na	0.018	0.246	0.085	0.270	0.014	0.221	0.034	0.275	0.079	0.282	0.176	0.271
K	0.000	0.060	0.015	0.060	0.002	0.050	0.000	0.060	0.010	0.090	0.060	0.090
Total A	0.018	0.306	0.100	0.330	0.016	0.271	0.034	0.335	0.089	0.372	0.236	0.361
Sum	15.073	15.306	15.100	15.330	15.053	15.271	15.034	15.335	15.089	15.372	15.236	15.361

Note: Fe^{3+} correction: (7A7W) cummingtonite host, all Fe^{2+}; cummingtonite lamella, (Si + Al) = 8; (Q-603C) cummingtonite host = 15 eNK; cummingtonite bulk host, 15 eNK; cummingtonite lamella, 14.925 eNK. For hornblende, see text. Oxides reported as weight percent.
* Calculated.

most samples is zoned between about An_{35} and An_{44}. The plagioclase in the orthopyroxene-bearing sample (HFW-307W) is An_{55}, and the plagioclase in sample Q-J44R is An_{22}. Garnets in 7A7R and 7A7C were nearly homogeneous and similar and had compositions of $Pyr_{19.3}Alm_{67.4}Sps_{3.3}Grs_{10.0}$ and $Pyr_{22.2}Alm_{66.0}Sps_{2.1}Grs_{9.7}$, respectively. The coexisting amphiboles of the CM series have a much wider range of X_{Mg} compared with those of the 7A7 series. Sample 7A7W and all samples of the CM series apparently are too rich in Mg and too poor in Al to coexist with garnet. The hornblendes of samples HFW-307W and Q-J44R plot differently than the other hornblendes. The hornblende of HFW-307W has a low Al content (9.5 wt% Al_2O_3), whereas the hornblende of Q-J44R shows a higher Na content (2.09 wt% Na_2O). Both of these chemical traits would cause the hornblende to plot more negatively on the projection (Fig. 3) and may reflect differences in the bulk chemistry of these two samples.

CHARACTERISTICS OF THE EXSOLUTION LAMELLAE

Orientation of the lamellae

In the petrographic microscope, all the clinoamphiboles showed extensive exsolution (Fig. 4). The coarsest visible lamellae are 2.5–1 μm wide and generally show a "100" orientation. The range of thicknesses for various exsolution orientations is given in Tables 2 and 3.

Samples of 7A7R, Q-603C, and Q-798M were oriented in the TEM so that the a^*-c^* plane lay perpendicular to the electron beam, and thus lamellae were exactly parallel to the electron beam. In this orientation, the angles between the lamellae and the a or c axis as well as the

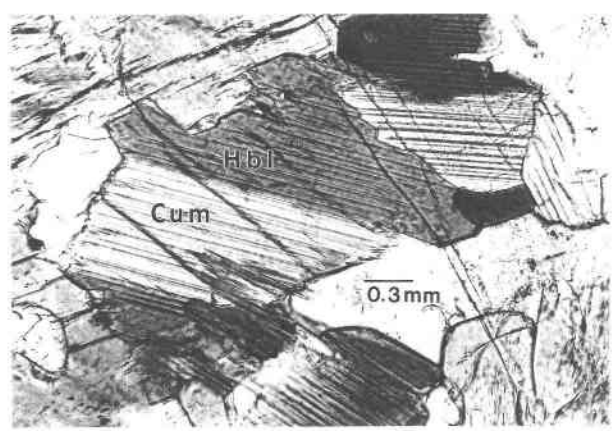

FIGURE 4. Photomicrograph of sample 7A7R that shows intergrown and extensive exsolution of clinoamphiboles. Coarsest visible lamellae are up to 2.5 μm thick.

TABLE 2. Angles (°) between "100" lamella and the *c* axis of the host phase and the average lamella thickness for samples Q-603C, Q-798M, and 7A7R

Q-603C						
Avg. "100" Lam ∧ c_{Cum} (°)	n.m.	0.0	n.m.	1.5	3.5	4.0
Avg. lamella thickness (μm)	~2.0	0.6	~0.4	0.03	0.01	0.009
Avg. "100" Lam ∧ c_{Hbl} (°)	n.m.	0.0	1.0	0.0	0.0	
Avg. lamella thickness (μm)	~2.0	0.76	0.18	0.08	0.005	
Q-798M						
Avg. "100" Lam ∧ c_{Hbl} (°)	n.m.	2.5	3.0	3.0		
Avg. lamella thickness (μm)	~1.7	0.42	0.02	0.002		
7A7R						
Avg. "100" Lam ∧ c_{Cum} (°)	n.m.	n.m.	2.0			
Avg. lamella thickness (μm)	~2.0	~0.6	0.1			
Avg. "100" Lam ∧ c_{Hbl} (°)	n.m.	n.m.	0.0	2.5		
Avg. lamella thickness (μm)	~1.7	~0.5	0.15	0.08		

Note: n.m. = not measured.

TABLE 4. Distances between "100" lamellae with similar thicknesses for samples 7A7D and Q-603C

7A7D		Q-603C	
Avg. "100" lamella width (μm)	Avg. distance (μm)	Avg. "100" lamella width (μm)	Avg. distance (μm)
1.05	10.5	1.50	12.50
0.60	1.65	0.75	7.00
0.04	0.37	0.46	1.10
		0.04	0.50
		0.003	0.02

lamellar width could be accurately measured. The orientations and widths of lamellae correlate and define natural groups of lamellae, which we interpret to be different generations or stages of exsolutions. These data are shown in Table 2 for the "100" lamella and the host's *c* axis ("100" ∧ *c*) and in Table 3 for the "10$\bar{1}$" lamella and the host's *a* axis ("10$\bar{1}$" ∧ *a*) for samples 7A7R, Q-603C, and Q-798M. In each case, the lamellae exsolved at higher temperatures are coarser than the lamellae exsolved at lower temperatures because of the correlation between diffusion rate and temperature. An obvious difference between the lamellar orientations of these samples is that in sample 7A7R, the angles between the lamella and the host's *a* axis increase as lamellar widths decrease, whereas sample Q-603C shows the opposite trend. In sample Q-798M, the "10$\bar{1}$" lamellar orientation does not change as a function of observed lamellar width (discussed later).

The "10$\bar{1}$" lamellar orientations can vary up to 4.1°, and differences of up to 4.0° are found for the "100" lamellae (Tables 2 and 3). In sample Q-603C, the widths of "10$\bar{1}$" exsolution lamellae range from 2.4 to 0.005 μm in cummingtonite, and the smallest of these lamellae are actually disc shaped. The cummingtonite lamellae in hornblende range from 1.5 to 0.18 μm. In sample 7A7R, "10$\bar{1}$" lamellar widths range from 1.5 to 0.1 μm in cummingtonite and from 1.5 to 0.1 μm in hornblende. For sample Q-798M, the observed hornblende "10$\bar{1}$" lamellar widths range from 1.0 to 0.07 μm.

Lamellar generations

For the amphiboles of samples 7A7R and Q-603C, several lamellar generations can be distinguished on the basis of their orientations and widths (Tables 2 and 3). However, several problems were inherent to the characterization of the lamellar generations. Not every measurable amphibole could be oriented with the electron beam parallel to the *b* axis in the TEM. As a consequences, the angle of the lamellae to the *a* or *c* axes of the hosts could not be measured in all cases, and these lamellae are identified by "n.m." in Tables 2 and 3. Most of the lamellar generations that are listed in Tables 2 and 3 are based on both lattice orientation and lamellar width, but several generations were identified only on the basis of lamellar width. Further, because only a very small area of the ion-milled sample could be observed in the TEM, it is still possible that additional lamellar generations are present elsewhere in these samples.

Interlamellar spacings of the lamellae assigned to different generations were measured for samples 7A7D and Q-603C (Table 4), and these spacings also support the existence of different lamellar generations (Schumacher et al. 1993). On the basis of all these data, sample 7A7R (7A7 series) showed at least three lamellar orientations,

TABLE 3. Angles (°) between "10$\bar{1}$" lamella and the *a* axis of the host phase and the average lamella thickness for samples Q-603C, Q-798M, and 7A7R

Q-603C								
Avg. "10$\bar{1}$" Lam ∧ a_{Cum} (°)	33.0	n.m.	31.8	n.m.	31.1	30.6	30.1	28.9
Avg. lamella thickness (μm)	2.4	~0.5	0.26	~0.13	0.05	0.03	0.01	0.005
Avg. "10$\bar{1}$" Lam ∧ a_{Hbl} (°)	n.m.	n.m.	30.9	30.2				
Avg. lamella thickness (μm)	~1.5	~0.45	0.24	0.18				
Q-798M								
Avg. "10$\bar{1}$" Lam ∧ a_{Hbl} (°)	31.0	31.0	31.0	31.0	31.0			
Avg. lamella thickness (μm)	1.0	0.45	0.15	0.07	0.005			
7A7R								
Avg. "10$\bar{1}$" Lam ∧ a_{Cum} (°)	n.m.	n.m.	31.9	32.6	33.9			
Avg. lamella thickness (μm)	~1.5	~0.45	0.27	0.15	0.10			
Avg. "10$\bar{1}$" Lam ∧ a_{Hbl} (°)	n.m.	32.0	32.5	33.9				
Avg. lamella thickness (μm)	~1.5	0.5	0.3	0.1				

Note: n.m. = not measured.

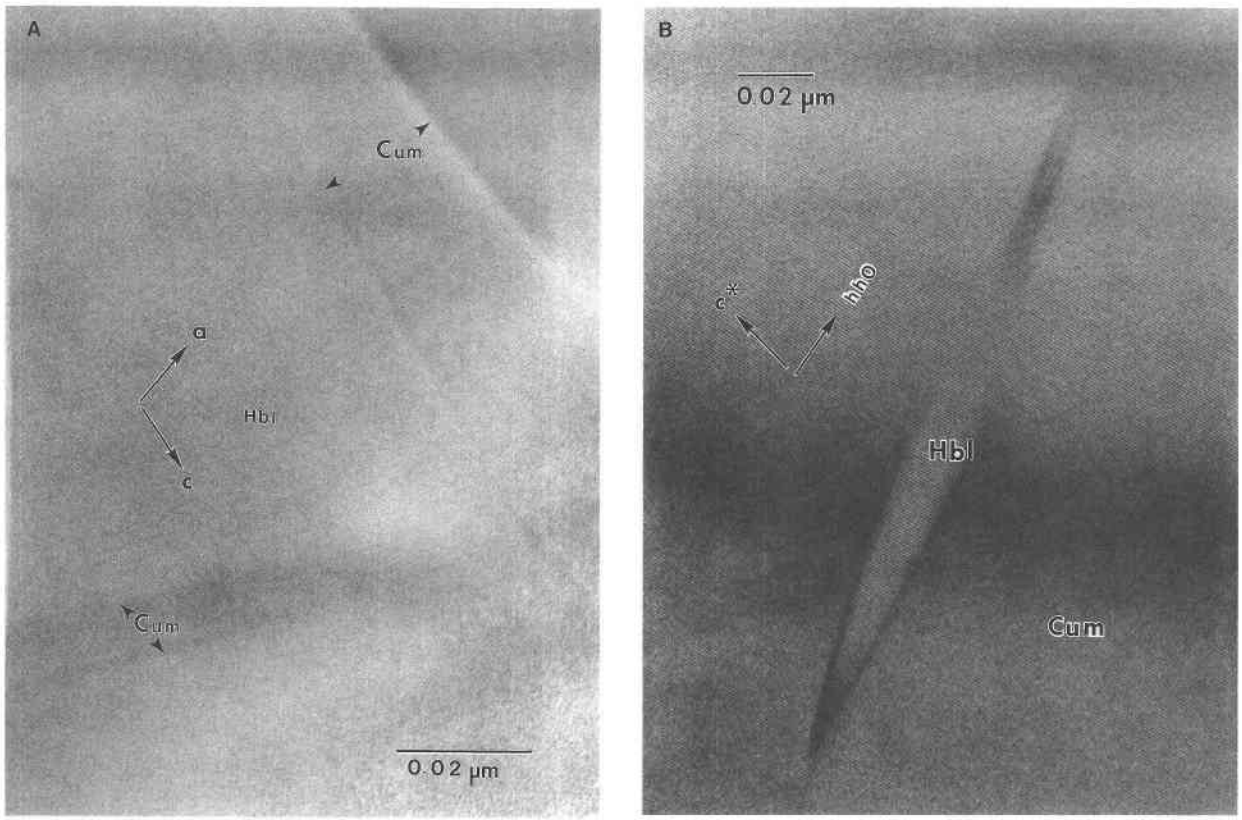

FIGURE 5. (A) HRTEM image of sample WD-H26C showing the coherent intergrowth between hornblende (Hbl) host and cummingtonite (Cum) exsolution lamellae. (B) HRTEM image of sample Q-603C showing the coherent intergrowth between cummingtonite host and "10$\bar{1}$" hornblende disc-shaped exsolution lamella viewed along [1$\bar{1}$0].

and sample Q-603C (CM series) showed at least six generations of exsolution lamellae.

HRTEM images

High-resolution TEM (HRTEM) images (Fig. 5) show the coherent intergrowths of the host and guest phases. Figure 5A is viewed down [010] onto the *a*-*c* plane, showing an intergrowth between hornblende host and "100" and "10$\bar{1}$" cummingtonite lamellae of sample WD-H26C. The interface between the host and the lamellae is very sharp, so in this orientation the electron beam is parallel to the lamellar interfaces. The "100" lamella shares the a^* axis with the host, and the c axis is common for the lamella and host. The "100" lamella shows a bending of the (001) fringes. The {10$\bar{1}$} lamella shares the c^* axis with the host, and the a axis is common for the lamella and host. Where the lamellae approach each other, one always tapers down to a point at the end, possibly because of strain-field interactions (Livi and Veblen 1989; Smelik and Veblen 1991). The "100" lamella shows bowing at the area were the two lamellae meet. The bowing feature is very common where lamellae approach one another (Smelik and Veblen 1993). A possible explanation is that the Ca in these regions diffuses to or away from the site of the "100" lamella because Ca diffusion is faster parallel to the Si double chains (parallel to the c axis).

Figure 5B shows the (110) adjustment of cummingtonite host and disc-shaped, "10$\bar{1}$" hornblende lamellae in sample Q-603C. The adjustment of the two coherent intergrown lattices by a slight rotation of the (110) lattice fringes is very conspicuous. Compositions of these lenticular lamellae and the host were compared qualitatively in the TEM by energy-dispersive X-ray analysis. A significant difference was detected between the Ca contents of the host and the lamellae. Additionally, electron spectroscopic imaging (ESI) of these disc-shaped exsolution lamellae (Czank et al. 1993) showed significant relative differences between the Ca contents of the guest and host phases. Hornblende lamellae were also found inside an approximately 2 μm wide, early cummingtonite lamella within a hornblende host (sample 7A7D). This feature is further evidence that these amphiboles actually underwent multiple phases of exsolution.

OPTIMAL PHASE-BOUNDARY CALCULATIONS

Influence of lattice parameters on lamellar orientation

According to optimal phase-boundary (OPB) calculations, the differences between the pairs of lattice parameters of the host and exsolved phase control the lamellar orientation (i.e., the temperature dependence of Δa, Δc, and $\Delta\beta$, where $\Delta a = a_{\text{host}} - a_{\text{lamella}}$, $\Delta c = c_{\text{host}} - c_{\text{lamella}}$, and $\Delta\beta = \beta_{\text{host}} - \beta_{\text{lamella}}$). To determine the contribution of the

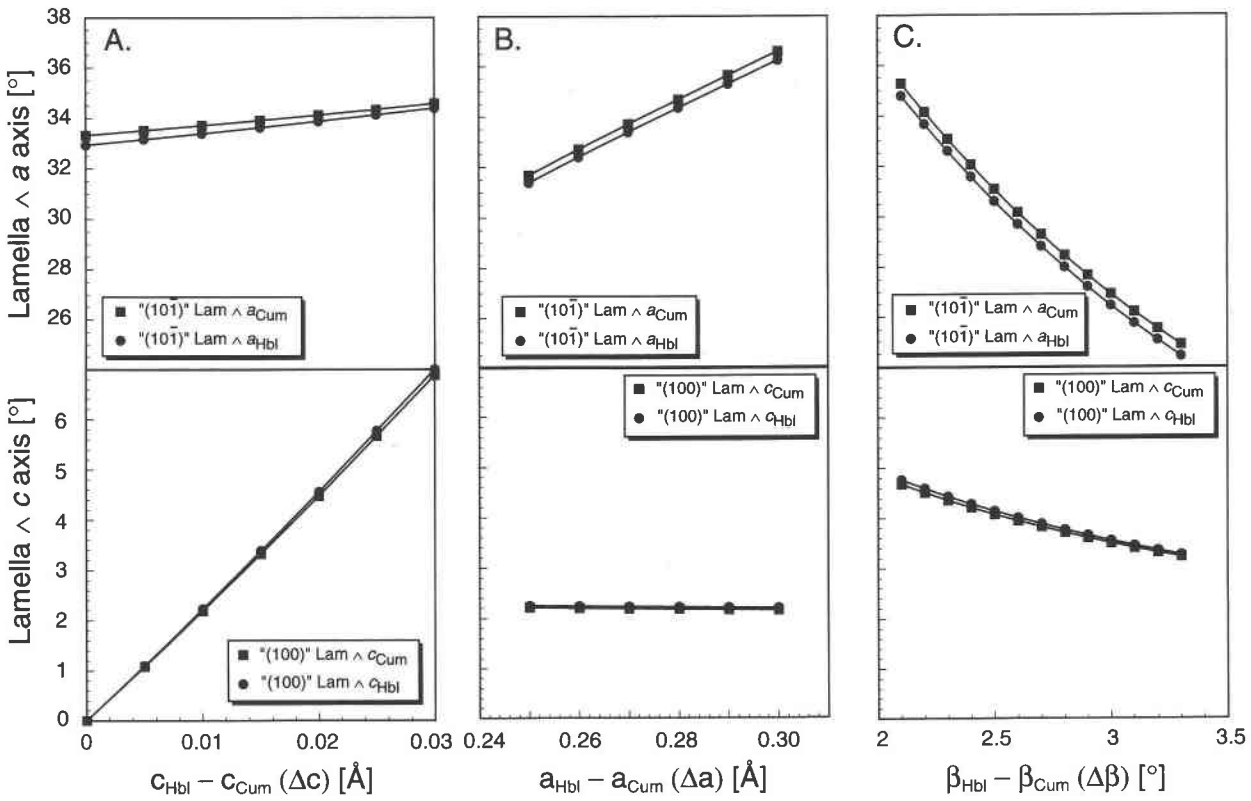

FIGURE 6. OPB calculations with constant a and β **(A)**, constant c and β **(B)**, and constant a and c **(C)**. Lattice parameters used are a_{Cum} = 9.54 Å, c_{Cum} = 5.35 Å, β_{Cum} = 102.22°, a_{Hbl} = 9.81 Å, c_{Hbl} = 5.35 Å, and β_{Hbl} = 104.67°.

parameters Δa, Δc, and $\Delta\beta$ to lamellar orientation, two parameters were held constant and the third was varied in the calculation (Fig. 6).

The "100" lamellar orientation is most strongly affected by the differences in the c lattice parameter (Δc) of the coexisting clinoamphiboles (Fig. 6A). A difference of only 0.03 Å between the two c lattice parameters of host and guest phase would change the relative orientation of the lamellae by 7°. Differences in the monoclinic angle ($\Delta\beta$) and a lattice parameter (Δa) have a lesser effect on the orientation of the "100" lamella.

Figure 6C shows unambiguously that the "10$\bar{1}$" orientation is most strongly affected by $\Delta\beta$. The Δa parameter has a smaller and opposite effect on the "10$\bar{1}$" orientation of the lamella (Fig. 6B). Variation of the c lattice parameter has practically no influence on the orientation of the "10$\bar{1}$" exsolution lamella.

Variations in lattice parameters with temperature

The temperature dependence of the amphibole lattice parameters was obtained by measuring d values with a Guinier film camera over a T range of 25–600 °C (Fig. 7). Figures 7A and 7B show different T-dependent changes in the lattice parameters of samples 7A7R and Q-603C, respectively, and indicate that the relative rates of change were not uniform. As a result, upon cooling, coherency strain must increase between lamella and host, but no features that can be attributed to this strain were observed.

The data on the T dependence of lattice parameters combined with the OPB theory allow the prediction of lamellar orientations for both the "10$\bar{1}$" and "100" lamellae at a certain temperature for samples 7A7R and Q-603C. However, the "100" lamellar orientation is clearly the least reliable of the two lamellar orientations because it strongly depends on the temperature variations of the c lattice parameters (Fig. 6), which are relatively small and the least certain of the measurements (Fig. 7). As a consequence, the rest of the discussion focuses on the temperature dependence of the "10$\bar{1}$" lamellar orientations.

Variations in lamellar orientation with temperature

For the amphiboles in Q-603C, the angle between the "10$\bar{1}$" lamellae and the a axis of the host increases with higher temperature, whereas, surprisingly, the same angle decreases with higher temperature in 7A7R (Table 3). This result is somewhat unexpected because the lattice parameters of all the amphiboles showed the same general changes with temperature (Fig. 7). This feature, however, results from different rates of change with temperature between the two samples in the Δa and $\Delta\beta$ of the

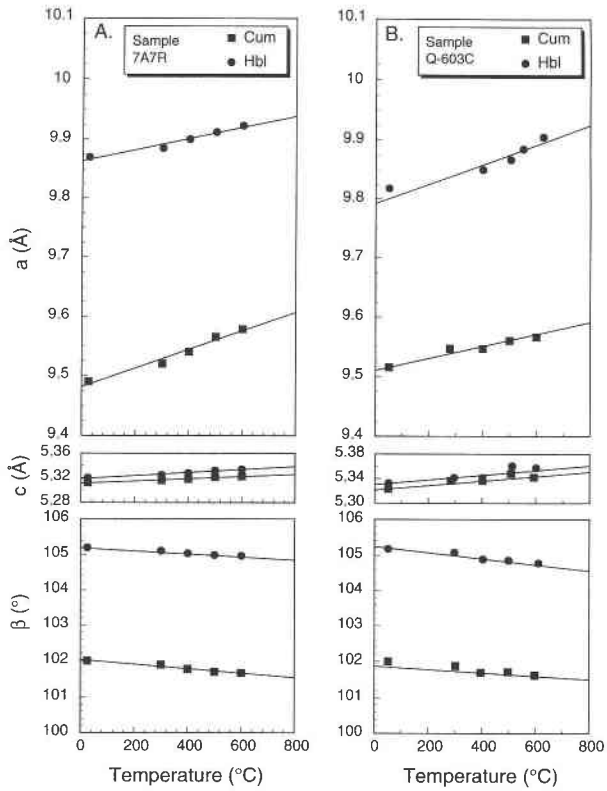

FIGURE 7. Temperature dependence of amphibole lattice parameters for sample 7A7R (**A**) and sample Q-603C (**B**). Lattice-parameter regression functions are as follows, in order of T: For 7A7R, $a_{Cum}(T) = 1.574 \times 10^{-4}T + 9.481(5)$, $c_{Cum}(T) = 1.807 \times 10^{-5}T + 5.311(2)$, $\beta_{Cum}(T) = -6.131 \times 10^{-4}T + 102.03(2)$, $a_{Hbl}(T) = 9.3573 \times 10^{-5}T + 9.864(6)$, $c_{Hbl}(T) = 2.501 \times 10^{-5}T + 5.318(2)$, $\beta_{Hbl}(T) = -4.224 \times 10^{-5}T + 105.19(2)$; and for Q-603C, $a_{Cum}(T) = 1.014 \times 10^{-4}T + 9.510(6)$, $c_{Cum}(T) = 3.652 \times 10^{-5}T + 5.321(2)$, $\beta_{Cum}(T) = -4.593 \times 10^{-4}T + 101.87(2)$, $a_{Hbl}(T) = 1.656 \times 10^{-4}T + 9.792(6)$, $c_{Hbl}(T) = 3.826 \times 10^{-5}T + 5.330(2)$, $\beta_{Hbl}(T) = -8.580 \times 10^{-4}T + 105.25(2)$. Errors given are indicated by parentheses and are based on averages of all measurements at different temperatures.

host and exsolved (lamellar) amphiboles. In Figure 7, values of a and β converge slightly in sample 7A7R, whereas these same values diverge slightly for sample Q-603C with increasing temperature. This feature is more clearly shown on plots of Δa vs. T and $\Delta\beta$ vs. T (Figs. 8A and 8B). The Δa and $\Delta\beta$ values are two key parameters in the OPB equation, and their contrasting behavior is the explanation for opposite trends that were observed in the angles between the "$10\bar{1}$" lamellae and the a axis as a function of temperature for the two samples. The property that probably controls the temperature dependence of Δa and $\Delta\beta$ values is composition, but, at present, too few data exist to quantify the compositional effects.

The variations in Δa and $\Delta\beta$ that are shown in Figure 8 suggest the possibility of exsolved amphiboles in which the Δa and $\Delta\beta$ are nearly independent of temperature (i.e., multiple generations of exsolution are roughly parallel).

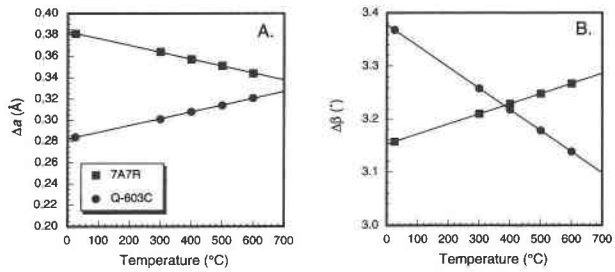

FIGURE 8. Variation of the differences in lattice parameters with temperature for cummingtonite and hornblende from samples 7A7R and Q-603C. (**A**) $\Delta a = a_{Hbl} - a_{Cum}$ and (**B**) $\Delta\beta = \beta_{Hbl} - \beta_{Cum}$.

This would explain the observations in sample Q-798M of nearly constant "$10\bar{1}$" $\wedge$ a angles despite the presence of populations of lamellae with distinct ranges of widths.

Exsolution and exsolution temperatures

Both cummingtonite and hornblende begin to break down to pyroxenes and other anhydrous phases at upper amphibolite- to granulite-facies conditions. As a result, the crest and the flatter parts of their heterogeneous solvus are metastable. This in turn renders supersolvus hornblende-cummingtonite compositions metastable relative to the pyroxene-bearing assemblages. As a consequence, mutual miscibility of hornblende and cummingtonite is much more restricted, and it is much more unlikely that, upon cooling, the spinodal regions of the cummingtonite-hornblende solvus will be encountered.

The style of exsolution that is normally ascribed to spinodal decomposition (fine, wavy intergrowths) was not observed in this study. The exsolution textures that have been described above are consistent with the overstepping of a coherent solvus and the precipitation and growth of new lamellae.

The scenario proposed is that, initially, homogeneous and coexisting cummingtonite and hornblende cooled below the coherent solvus. Subsequent intervals of undercooling resulted in various stages of coherent exsolution until at lower temperatures the kinetics became too sluggish for exsolution to continue. To reconstruct partially the exsolution history, the T dependence of the lattice parameters (a and β) and OPB theory were used to calculate plots of "$10\bar{1}$" lamella $\wedge a_{host}$ vs. temperature for samples 7A7R and Q-603C (calibration curves in Fig. 9). The actual measured orientations were then plotted, and the temperatures of exsolution were derived (Figs. 9A and 9B). The estimated exsolution temperatures are between 780 and 300 °C for both samples with an error of ±80 °C, which is based on the maximum errors of the lattice parameters that were used to construct the calibrations curves.

The highest exsolution temperature of 780 °C for the first generation of exsolution in Q-603C is the only estimate that lies above independent estimates of peak metamorphic temperatures. However, use of the maximum

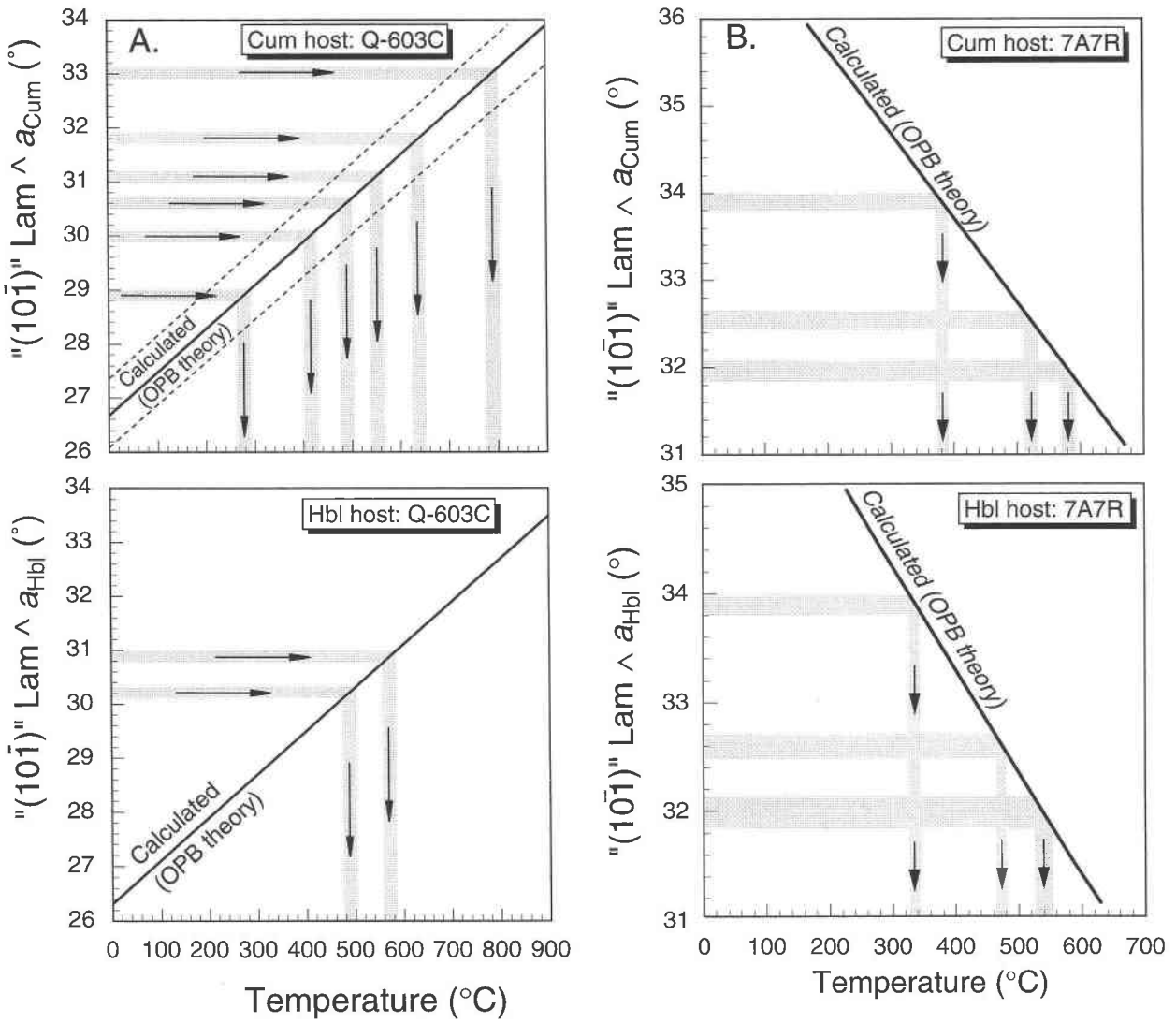

FIGURE 9. Derivation of the exsolution temperatures for sample Q-603C (**A**) and sample 7A7R (**B**). The width of the shaded lines indicates the errors (±0.1°) associated with measuring the lamellar angles. The solid line is the theoretical variation of lamellar angle with T given by the optimal phase boundary (OPB) calculations. The dashed lines indicate the uncertainty in the determinations of the variation of the lattice parameters with T. (See also Tables 2 and 3.)

error of the lattice parameters for the determination of the OPB calibration curve indicates that the temperature of exsolution could have been as low as 700 °C (Fig. 9A). This is very close to and probably within the error of the estimated peak metamorphic temperatures of 675 °C for locality Q-603C, which reached temperatures near the breakdown of muscovite + quartz in associated pelitic rocks. It should also be noted that estimates of exsolution temperatures above 600 °C are based on linear extrapolations of the temperature dependence of the lattice-parameter data well beyond the temperature range of the measurements. If the extrapolations are not valid for higher temperatures, this could explain the unreasonably high temperature of exsolution for the first generation of exsolution. Consequently, the temperatures that are assigned to events that are above about 650 °C are more speculative, although the sequence of events that is outlined below must have occurred.

These results suggest the following sequence of events for both localities. At or around peak metamorphic temperatures the assemblages contained two homogeneous amphiboles, hornblende and cummingtonite. (In the optical microscope, epitaxial intergrowth of hornblende and cummingtonite parallel to {10$\bar{1}$} and {100} was common.) For sample Q-603C, the first hornblende exsolution lamellae (~2.4 μm wide) in cummingtonite must have formed slightly below peak metamorphic conditions. Further exsolution of the cummingtonite host formed hornblende lamellae that were about 0.5 μm thick (lamellar orientation and, therefore, T could not be de-

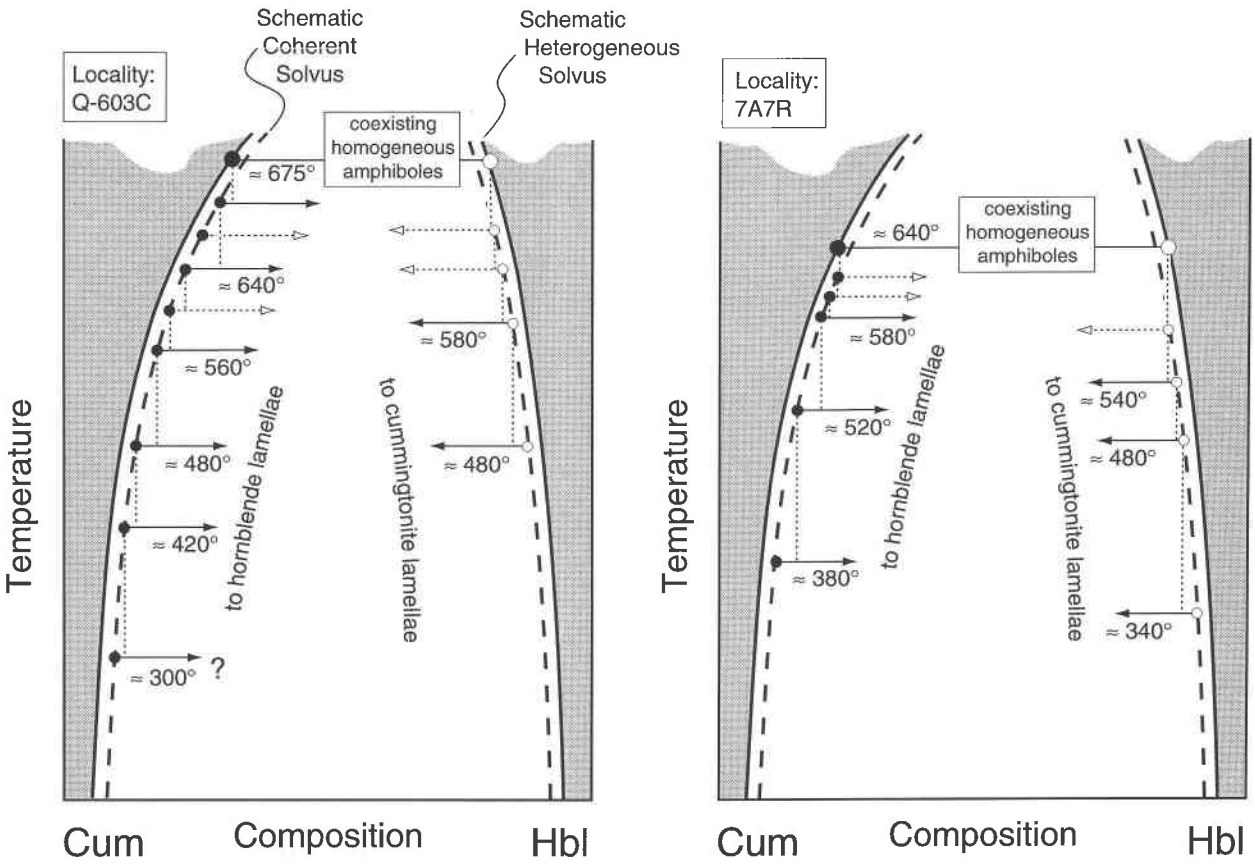

FIGURE 10. A schematic cummingtonite-hornblende solvus that summarizes the exsolution histories of samples Q-603C and 7A7R. Solid lines with arrowheads indicate that exsolution generation was characterized by both lamellar angle and average lamellar width; dashed lines with arrowheads indicate that the exsolution generation could only be characterized by average lamellar width (lamellar angle could not be measured). See text for discussion.

termined). A third phase of hornblende exsolution occurred at about 640 °C (0.26 μm). Lamellar size (0.13 μm) suggests an additional hornblende generation between 640 and 560 °C. These were followed by successive generations of hornblende lamellae formed at about 560, 480, 420, and 300 °C (Figs. 9A and 10, Table 3).

The lowest exsolution temperatures of about 300 °C were derived from the nanometer-sized, disc-shaped, hornblende exsolution in the cummingtonite host of sample Q-603C. Because these exsolutions do not have straight boundaries, their orientation cannot be measured accurately, so this temperature of exsolution is tentative at best. Additionally, the OPB theory may no longer be describing exsolution at these temperatures and with these dimensions.

Hornblende in sample Q-603C exsolved two generations of cummingtonite (thicknesses of about 1.5 and 0.45 μm) that could not be measured but must have formed above about 580 °C (Fig. 10). Two generations of cummingtonite lamellae formed at about 580 and 480 °C (Figs. 9A and 10, Table 3).

The cummingtonite of sample 7A7R exsolved two generations of hornblende (thicknesses of about 1.5 and 0.45 μm) that could not be measured but must have formed between about 580 °C and the peak metamorphic temperature of about 640 °C. Three additional generations of hornblende lamellae formed at about 580, 520, and 380 °C.

The earliest generation of cummingtonite lamellae in hornblende from sample 7A7R could not be measured (thickness of about 1.5 μm) but must have formed between 640 and 540 °C. Three generations of cummingtonite exsolution are found in hornblende of 7A7R, and these occurred during cooling at about 550, 480, and 340 °C (Figs. 9B and 10).

These two multigenerational exsolution histories are consistent with the evidence that the histories (P-T paths) for the two localities are different (e.g., Schumacher et al. 1989). The observations here suggest that amphibolite rocks of the CM series (Q-603C) cooled more slowly than amphibolite rocks of the 7A7 series (7A7R) (Schumacher et al. 1993).

Given the present state of our understanding of the thermal, baric, and compositional control of hornblende and cummingtonite lattice parameters, a general hornblende-cummingtonite geothermometer is not presently

feasible. However, we have shown that detailed study of individual samples can produce results that can be predicted with OPB theory. As more amphibole data become available, routine determination of temperatures of exsolution in cummingtonite and hornblende may become possible.

Acknowledgments

We thank S. Malinowski and T. Ahrens of the CEM-Institut in Neumünster, Germany, for the use of their ion milling apparatus. We are grateful to T. Sharp, F. Seifert, and A. Hogrefe for the opportunity to prepare TEM samples at the Bayrisches Geoinstitut, Bayreuth, Germany. T. Sharp improved this paper by fruitful discussions and comments. B. Mader and D. Ackermand provided valuable assistance during microprobe work. H. Unger and K. Fesenmeier are thanked for the preparation of excellent thin sections. Special thanks go to K. Hollocher for supplying samples and to P. Robinson and E. Smelik for helpful discussion and suggestions. We also thank D.R. Veblen and D.R. Peacor, whose comments greatly improved the presentation. This work was supported by the Deutsche Forschungsgemeinschaft (DFG) grant number Cz 19/4-1 to M.C. and J.C.S., and the collection of some of the sample material was supported by NATO Cooperative Research Grant 0374/87 to J.C.S., P. Robinson, and M.C.

References cited

Asklund, B. (1923) Petrological studies in the neighborhood of Stavsjö at Kilmärten. Sveriges Geologiska Undersökning, 17(6), 122 p.

Asklund, B., Brown, W.L., and Smith, J.V. (1962) Hornblende-cummingtonite intergrowths. American Mineralogist, 47, 160–163.

Binns, R.A. (1965) The mineralogy of metamorphosed basic rocks from Willyama Complex, Broken Hill District, New South Wales: Part I. Hornblendes. Mineralogical Magazine, 35, 306–326.

Bollman, W., and Nissen, H.-U. (1968) A study of optimal phase boundaries: The case of exsolved feldspars. Acta Crystallographica, A24, 546–557.

Boriani, A., and Minutti, L. (1965) La cummingtonite di Ornavasso. Rendiconti Istituto Lombardo di Scienze e Lettere. A scienze matematiche, fisiche, chimiche e geologiche, 99, 412–424.

Calleghari, E. (1965–66) Osservazioni su alcune cummingtonite del massiccio dell'Adamello. Memorie Accademia Patavina, Classe di Scienze Matematiche e Naturali, 78, 273–310.

Cameron, M., Sueno, S., Prewitt, C.T., and Papike, J.J. (1973) High-temperature crystal chemistry of acmite, diopside, hedenbergite, jadite, spodumene, and ureyite. American Mineralogist, 58, 594–618.

Cameron, M., and Papike, J.J. (1979) Amphibole crystal chemistry: A review. Fortschritte der Mineralogie, 57, 28–67.

Czank, M., Klein, U., Mayer, J., and Schumacher, J.C. (1993) Anwendung der elektronenmikroskopischen Abbildung (ESI) zum Nachweis von Entmischungen im Nanometermaßstab Beihefte zum. European Journal of Mineralogy, 5, 149.

Fleet, M.E. (1982) Orientation of phase and domain boundaries in crystalline solids. American Mineralogist, 67, 926–936.

——— (1985) Orientation of phase and domain boundaries in crystalline solids: Reply. American Mineralogist, 70, 130–133.

Hollocher, K.T. (1985) Geochemistry of metamorphosed volcanic rocks in the Middle Ordovician Partridge Formation, and amphibole dehydration reactions in the high-grade metamorphic zones of central Massachusetts (contribution no. 56). Ph.D. thesis, University of Massachusetts, Amherst.

——— (1993) Geochemistry and origin of volcanics in the Ordovician Partridge Formation, Bronson Hill anticlinorium, west-central Massachusetts. American Journal of Science, 293, 671–721.

Hovestreydt, E.R. (1983) FINAX: A computer program for diffraction angles, refining cell parameters and calculating powder patterns. Journal of Applied Crystallography, 16, 651–653.

Jaffe, H.W., Robinson, P., and Klein, C. (1968) Exsolution lamellae and optic orientation of clinoamphiboles. Science, 160, 776–778.

Livi, K.J.T., and Veblen, D.R. (1989) Transmission electron microscopy of interfaces and defects in intergrown pyroxenes. American Mineralogist, 74, 1070–1083.

Robinson, P. (1963) Gneiss domes of the Orange area, Mass. and N.H. Ph.D. dissertation, Harvard University, Cambridge, Massachusetts.

——— (1986) The central Massachusetts metamorphic high. In P. Robinson and D.C. Elbert, Eds., Regional metamorphism and metamorphic phase relations in northwestern and central New England: Field trip guidebook (B-5), 14th General Meeting, International Mineralogical Association, 1–10.

Robinson, P., and Jaffe, H.W. (1969) Chemographic exploration of amphibole assemblages from central Massachusetts and southwestern New Hampshire. Mineralogical Society of America Special Paper, 2, 251–274.

Robinson, P., Jaffe, H.W., Ross, M., and Klein, C., Jr. (1971) Orientations of exsolution lamellae in clinopyroxenes and clinoamphiboles: Consideration of optimal phase boundaries. American Mineralogist, 56, 909–939.

Robinson, P., Ross, M., Nord, G.L., Jr., Smyth, J.R., and Jaffe, H.W. (1977) Exsolution lamellae in augite and pigeonite: Fossil indicators of lattice parameters at high temperatures and pressure. American Mineralogist, 62, 857–873.

Robinson, P., Spear, F.S., Schumacher, J.C., Laird, J., Klein, C., Evans, B.W., and Doolan, B.L. (1982a) Phase relations of metamorphic amphiboles: Natural occurrence and theory. In Mineralogical Society of America Reviews in Mineralogy, 9B, 1–211.

Robinson, P., Tracy, R.J., Hollocher, K.T. Dietsch, C., and Berry, H.N. (1982b) High grade Acadian regional metamorphism in south-central Massachusetts. In R.A. Joesten and S.S. Quarrier, Eds., Guidebook for field trips in Connecticut and south-central Massachusetts. State Geological and History Survey of Connecticut Guidebook, 15, 289–339.

Robinson, P., Tracy, R.J., Hollocher, K.T., Schumacher, J.C., and Berry, H.N. (1986) The central Massachusetts metamorphic high. In P. Robinson and D.C. Elbert, Eds., Regional metamorphism (B-5), 14th General Meeting, International Mineralogical Association, 195–234.

Robinson, P., Thompson, P.J., and Elbert, D.C. (1991) The nappe theory in the Connecticut Valley region: Thirty-five years since Jim Thompson's first proposal. American Mineralogist, 76, 689–712.

Ross, M., Papike, J.J., and Shaw, K.W. (1969) Exsolution textures as indicators of subsolidus thermal histories. In Mineralogical Society of America Special Papers, 2, 275–299.

Schumacher, J.C. (1988) Stratigraphy and geochemistry of the Ammonoosuc Volcanics, central Massachusetts and southwestern New Hampshire. American Journal of Science, 288, 619–663.

——— (1991) Empirical ferric iron corrections of electron microprobe mineral analyses: Necessity, assumptions, and effects on some geothermometers and geobarometers. Mineralogical Magazine, 55, 3–18.

Schumacher, J.C., Schumacher, R., and Robinson, P. (1989) Acadian metamorphism in central Massachusetts and south-western New Hampshire: Evidence for contrasting *P-T* trajectories. In J.S. Daly, R.A. Cliff, and B.W.D. Yardley, Eds., Evolution of metamorphic belts, p. 453–460. Geological Society Special Publication no. 43.

Schumacher, J.C., Klein, U., and Czank, M. (1993) Temperatures of mutual exsolution in hornblende and cummingtonite as possible evidence for varying regional metamorphic cooling rates. Geological Society of America Abstracts with Programs, 25, A101.

Seitasaari, J. (1952) An association of cummingtonite and hornblende. Annales Academiae Scientiarum Fennicae Series A., III. Geologica Geographica, 30, 5–20.

Smelik, E.A., and Veblen, D.R. (1991) Exsolution of cummingtonite from glaucophane: A new orientation for exsolution lamellae in clinoamphiboles. American Mineralogist, 76, 971–984.

——— (1993) A transmission and analytical electron microscope study of exsolution microstructures and mechanisms in the orthoamphiboles anthophyllite and gedrite. American Mineralogist, 78, 511–532.

Smith, J.V. (1969) Crystal structure and stability of Mg_3SiO_3 polymorphs; physical properties and phase relations of Mg, Fe pyroxenes. Mineralogical Society of America Special Paper, 2, 3–29.

Smyth, J.R. (1974) The high temperature crystal chemistry of clinohypersthene. American Mineralogist, 59, 1069–1082.

Stout, J.H. (1972) Phase petrology and mineral chemistry of coexisting amphiboles from Telemark, Norway. Journal of Petrology, 13, 99–146.

Thompson, J.B., Jr. (1978) Biopyriboles and polysomatic series. American Mineralogist, 63, 239–249.

Tracy, R.J., Robinson, P., and Thompson, A.B. (1976) Garnet composition and zoning in the determination of temperature and pressure of metamorphism, central Massachusetts. American Mineralogist, 61, 762–775.

Vernon, R.H. (1962) Co-existing cummingtonite and hornblende in an amphibolite from Duchess, Queensland, Australia. American Mineralogist, 47, 360–370.

Whittaker, E.J.W., and Zussman, J. (1961) The choice of axes in amphiboles. Acta Crystallographica, 14, 54–55.

Yang, H., and Hirschmann, M.M. (1995) Crystal structure of $P2_1/m$ ferromagnesian amphibole and the role of cation ordering and composition in the $P2_1/m$-$C2/m$ transition in cummingtonite. American Mineralogist, 80, 916–922.

Manuscript received August 13, 1994
Manuscript accepted March 8, 1996